The structure and mechanical properties of Cu₅₀Ni₅₀ alloy nano-foams formed via polymeric templating

Chang-Eun Kim^{a,b}, Raheleh M. Rahimi^a and David F. Bahr^{a,*}

^aSchool of Materials Engineering, Purdue University, West Lafayette, IN 47906-2045,

USA

^bLawrence Livermore National Laboratory 7000 East Avenue, Livermore, CA 94550,

USA

Address all correspondence to David Bahr at dfbahr@purdue.edu

Abstract

We demonstrate multicomponent metallic alloy nano-foams can be synthesized by the polymeric templating method. The present approach enabled alloy compositions not accessible via commonly used de-alloying or co-deposition methods. We report the synthesis of a Cu₅₀Ni₅₀ alloy nano-foam using electrospinning polymeric templating, which exhibits distinct polycrystallinity, process-driven segregation, and enhanced mechanical strength over the pure Cu nano-foam. Transmission electron microscopy revealed microscopic grain formation and their slightly variable compositions. The processing method is applicable to the synthesis of wide ranges of multi-component metal porous materials, creating new research opportunities for noble alloy foams that were not available through the wet electrochemical routes.

Introduction

Metal nano-foams present special properties that are not commonly found in bulk metals. These architectures are made of mostly empty pores and thin ligaments, featuring very large surface area per unit volume. The high surface-to-bulk ratio of metal nano-foam has spurred interest in research towards catalysis, filtering, and other chemical processing. Their porous microstructure leads to challenges in determining the mechanisms which govern the mechanical strength of such extremely porous metals. Properties of the nanoporous metals that are closely related to surface properties, such as plasmonic response, optical absorption, phononic response and thermal properties, are impacted by the structure of the materials. Unfortunately, many of these research opportunities have been achieved for a few select elements. The most common methods of fabricating metal nano-foams — dealloying and co-deposition — rely on chemical mechanisms that are only suitable for a limited range of elements.

Dealloying typically begins with a binary bulk metals, from which the more reactive component is dissolved out, leaving the less reactive component in a porous microstructure.^{6,7} In this way, the available species of nano-foam is pre-determined by their electrochemical potentials.⁸ For example, if we begin with Cu-Ni binary alloy, the dealloying process will always favor Cu to remain as the foam body, because the electrochemical potential of Cu is lower (or Cu is more noble) than Ni. During dealloying process, the porosity of the foam changes along with the composition during the reaction, meaning that the structure and composition of the foam sample are not independent variables. Comparison between any two samples with different compositions makes it challenging to separate the composition dependence of the mechanical

strengthening effect from the porosity dependence due to its microstructure. In addition, relying on dissolution means it is difficult to obtain a high-purity unary metal nanofoam ^{9,10}

These three intrinsic limitations of dealloying method—limited choice of elements, intertwined structure/composition variables, and challenges in reaching high purity unary phase, can be avoided by using a new process noted as the electrospinning polymeric templating method. We have previously shown the third problem can be avoided by using this new process; in the current paper we address the issue of the first two challenges.¹¹

Another synthesis method for alloy nano-foams is the co-deposition method.¹² In co-deposition, for example the Cu-Ni alloy case, a very dilute Cu precursor is mixed with a rich Ni precursor in an electrochemical bath. At large current density during electroplating the more reductive Cu depletes first, creating a local opportunity to reduce Ni, until more Cu precursors are transported into the reaction zone. Therefore, the actual chemical composition of the final foam product is determined by mass transport of Cu ion, which does not necessarily scale to the amount of Ni in the electrochemical bath, and also depends on various factors: temperature, type of electrolytes, local geometry, and so on. The use of electrospinning polymeric template method can provide a much simpler way to accurately control the alloy composition of a metal nano-foam. We report an early example of this new process, detailing the unique structural property of the nano-foam obtained this way due to the segregation of intermediate oxide alloy.

An additional advantage of using electrospinning polymeric template method is the scalability of the fabrication. Electrospinning is a well-known technique to produce a large fabric of non-woven nanofibers.¹³⁻¹⁵

The target composition we chose in this work, Cu:Ni = 50:50, would be challenging to accurately control via dealloying or co-deposition methods. By the method we used in this work, the composition can be controlled by simply mixing the proper molarity of precursors into the electrospinning feedstock. In this way, the chemical composition is determined by the concentration of feedstock, while the foam structure is mainly controlled by the electrospinning process parameters. The rest of this article is dedicated to give proofs to this point, along with a few observational details.

Materials and Methods

The Cu₅₀Ni₅₀ alloy nano-foam was synthesized by a two-step thermal treatment of a non-woven electrospun fabric made out of a polyvinyl alcohol (PVA) and metal acetate (Ac) solution, hereby PVA–Cu(Ac)–Ni(Ac). The electrospinning was carried out using a Spellman SL 300 voltage controller and a syringe pump.¹⁵ The voltage was set to 15 kV, and the distance between syringe tip to the target surface was 12 cm. The target was made out of a sheet of thin copper (thickness 0.5 mm) wrapped on a 3D-printed plastic frame.

The PVA–Cu(Ac)₂–Ni(Ac)₂ electrospinning solution was prepared by mixing deionized water 16.8 g, polyvinyl alcohol (MW=124k-186k, Aldrich, 87-89% hydrolyzed) 1.68 g, copper(II) acetate monohydrate (Fisher Scientific Acros, ACS Reagent grade) 0.6 g and nickel(II) acetate tetrahydrate (Sigma-Aldrich, 99.998% trace metal basis) 0.75 g at room temperature. The mixture was loaded into a plastic syringe installed on the syringe pump. The pump speed was set to about 0.17 mL/h. The deposition was carried out for 90 minutes to create a patch of non-woven fabric. The electrospun fabric was dried in ambient atmosphere for 30 minutes, then was

mechanically detached from the foil, followed by subsequent two-step thermal treatments.

The first heat treatment was carried out to burn-off the PVA, using an initial ramping rate of 5 °C/min to 500 °C, dwell for 2 hours, followed by closed oven cooling. In this first heating process, the electrospun fabric undergoes thermal decomposition. We used thermogravimetric analysis (TGA) to find an inflection point at 196.5 °C of this procedure. The TGA was carried out by scanning from 25 °C to 500 °C at a ramping rate of 5 °C/min, using TGA-Q50 (TA instruments Inc.).

As a result of the first thermal process, an oxide nano-foam was created in which both copper oxide and nickel oxide coexist as identified by the x-ray diffraction (XRD). The XRD analysis was carried out using Bruker D8 equipped with Cu K- α (λ = 1.5406 Å) radiation source, using locked coupled scanning mode with a scanning rate of 5 deg./min.

The subsequent reducing thermal process for the oxide nano-foam was carried out under reducing gas (95% Ar, 5% H₂) flow in a quartz tube surrounded by optical radiation heat source. The temperature was measured by a thermocouple located near the sample. Before heating to 330 °C, the forming gas was flushed for 30 minutes at 40 sccm. The chosen temperature is slightly above the complete miscible point of the Cu-Ni binary phase. The heating lasted for 45 minutes. The reducing gas was kept flowing (40 sccm) while cooling to room temperature.

The morphology of the alloy nano-foam was examined using a FEI Quanta 650 electron microscope equipped with focused ion beam (FIB) column and lift-out probe (Omniprobe 200, Oxford instrument Inc.). A specimen for transmission electron microscopy (TEM) was prepared by using the FIB and lift-out probe. A $10\mu m \times 0.3 \mu m \times 10^{-2}$

5 μm slice of the metallic nano-foam was cut from the sample and implanted on a Mo grid post. The gallium (Ga) ion beam was used with variable voltage/current setting from 30 kV/20 nA to 30 kV/0.1 nA to shape the specimen and mount on the grid. The implanted sample underwent additional thinning down to about 100 nm in thickness using more gentle ion beam settings ranging from 30 kV/0.5 nA to 5 kV/ 0.05 nA. The transmission electron microscopy was carried out using a FEI Talos 200X TEM/STEM microscope, equipped with ChemiSTEM (X-FEG and four silicon drift EDS detectors), operated at 200 kV. The mechanical strength of the foam was assessed by nanoindentation using the Oliver-Pharr method. 17-19 A Hysitron Triboindenter 950 (Hysitron Bruker, Minneapolis MN) equipped with a 100 μm diameter flat punch tip was used to apply a partial loading-unloading method to measure the hardness of the nano-foam.

Results and Discussion

The Cu-Ni alloy nano-foam exhibits complex morphologies that evolve through the two-step heating processes. After the first heating, the oxides of Cu-Ni show granular segregations (Fig. 1 (a)). These segregations disappear after the second heating process in the reducing gas condition (Fig. 1 (b)). Through these oxidation and reduction heating processes, the size and shape of the ligaments vary significantly, where the ligaments of the final metal stage are about 50 % thinner than those of the oxide phase.

Energy dispersive spectroscopy (EDS) mapping revealed that the granular segregations are rich in copper (Fig. 2). But after the second heating process, chemical segregation is no longer visible in the micrometers length scale ((Fig. 2 (f, h)); and the x-ray diffraction (XRD) does not detect noticeable oxide peaks ((Fig. 2 (c, g)). The EDS

analysis determined Cu:Ni=53:47 by atomic ratio. Although the segregation is no longer apparent in the micrometers scale, more detailed analyses using transmission electron microscopy (TEM) revealed that microscopic segregation still persists.

High resolution SEM images show that there are many pits and humps on the surface of the alloy metal foam (Fig. 3). These rough features resemble those of pure Cu foams formed with this method (shown in Fig. 3).¹¹ The mechanical strength of the Cu-Ni alloy nano-foam is about three times stronger than that of a previously reported pure Cu nano-foam (Fig. 3).¹¹ Hardening with continued compression is a result of densification of the foam, and so the relative strength at a given depth (strain) of compression is an appropriate measure of increased strength between the systems.

The microstructure of this alloy nano-foam is polycrystalline (Fig. 4(a, b)) according to the TEM analyses. Interestingly the diffraction suggests that the chemical composition of each of the grains varies significantly (Fig. 4(c)). The lattice spacings of the Cu-Ni alloy metal nano-foam are determined from the diffraction pattern Fig. 4(b), which turns out to be smaller than that of Cu, and larger than that of Ni. The measured interlayer spacings are listed in Table S1 of the online supplementary material. A quantitative analyses and comparison of the EDS maps show that the alloy nano-foam still have significant level of heterogeneity in the composition distribution. (Fig. 4(d,e,f)), in agreement with the variation in alloy compositions as Fig. 4(c).

The current work demonstrates that it is possible to obtain metal alloy nano-foams via the electrospinning polymeric template method. There are several unique features of the resulting structures that are not observed in nanoporous metals formed via other nanofoam syntheses. First, the creation of an intermediate oxide segregation phenomena is a part of this process, which may in and of itself be a useful structure. Secondly, resulting Cu-Ni alloy seems almost homogeneous (Fig. 2) but TEM analyses found that more microscopic compositions still varies significantly (Fig. 4). The oxide phases, CuO and NiO, have different crystalline structures that are not miscible to each other, leading to phase segregation, as indicated by the granular Cu-rich oxide (Fig. 2). The segregation attenuates after the second thermal process under the reducing gas condition, due to intermetallic diffusion. We speculate that immiscibility of the intermediate oxides can be utilized to make interesting nanoscale structures, such as core-shell or ripening patterns.

For the case of Cu-Ni alloy, the two components are known to completely miscible.²⁰ But diverse range of elements can be used for this electrospinning template methods, suggesting much less compatible combinations, such as bcc/hcp metals might result in more segregated metal nano-foams. The oxide segregation phenomenon can be used as an advantage for nanostructuring syntheses.

The Vegard's law we used to determine alloy composition from the TEM diffraction pattern (Fig. 4(c)), deserves discussion.^{21, 22} The Vegard's law asserts that the lattice parameters of a miscible alloy can be expressed as a weighted average of the lattice parameters of the pure components, where those weights are atomic compositions. The current alloy system Cu-Ni satisfies the assumptions of this empirical law, and we chose this correlation to map the measured lattice parameters from TEM diffraction to the alloy compositions of each grain. The diffraction pattern was recorded by using spread (weak) electron beam and long exposure; and the astigmatism was carefully corrected in order to obtain precise patterns.

The results clearly demonstrate that the electrospinning templating method enables the synthesis of non-noble alloy metal foams, such as Cu₅₀Ni₅₀. The other advantage of the present process is to separate the morphology control from the composition control. Unlike dealloying or co-deposition methods, the microstructure of foam does not directly depend on the chemical composition. Instead, the structure of polymeric templates (electrospun fibers) are controlled by electrospinning equipment parameters. We did not demonstrate this idea in this work, but this advantage of the present process deserves an emphasis. Ideally, the composition control (by feedstock chemicals) can be independent from the morphology control (by equipment parameters). But we also stress that altering the composition of feedstock can change the optimal spinning parameters, as well. For example, we observed that higher Ni(Ac)₂ content can result in thinner spinning jet. We also noted that electrospinning parameters can drift by varying atmospheric conditions (humidity, temperature), which makes an air-conditioned chamber, though not used in the current work, will be needed for process parameter optimization.

The polycrystalline nature of the resulting Cu-Ni nano-foam is also unique and interesting. The dealloying or co-deposition methods produce more coherent (close to single crystalline) material. Dealloying method begins with well equilibrated alloy bulk, in which high energy grain boundaries can have enough time and thermal energy to rearrange. Dissolving process creates the pores, at the same time, it prompts unstable adatoms to rearrange, 7,23 leading to form an ordered structure. In co-deposition method, the interface energy can drive increased coherency between each new layer and the existing deposit. But in the electrospinning polymeric template method, the thermal decomposition of precursors can occur in a widely scattered fashion, creating many interfaces, but with little access to adjacent vacancies, due to confined volume in the nanoscale ligaments. Lattice vacancies enables rearrangement of the interface atoms via diffusion process, but their absence limits relaxation of the grain boundaries. The observed polycrystallinity stands because the forming mechanism is fundamentally different from dealloying or co-deposition methods.

The thermal decomposition of precursors can be a source of impurities. Interestingly our EDS mapping did not indicate significant presence of impurity species, for example, metal carbides. Solubility of carbon in those two metals are extremely low at benign temperature.²⁴ This useful property of Cu and Ni may have helped to remove carbon species generated from the decomposition of polymeric templates. For certain alloy components that have strong affinity to carbon species, for example W, Ti, Mo, and Ta, it is recommended to check if they formed carbide species during the thermochemical processes.

The alloy nano-foam in the present work showed much higher mechanical strength compared to pure Cu nano-foam but note that the strengthening should not be directly attributed to the alloying effect. The measured strength, in fact, represent the macroscopic response of the metal nano-foam film, which has more variables other than strength of the material that consists the ligaments. There are mathematical models to relate the macroscopic strength of a foam to the strength of individual ligament. For example, Ashby has pioneered in this area.²⁵ In this context, the present nano-foam can be classified as an open-cell type nano-foam film. But considerable irregularity among the ligaments makes it harder to apply the idealized models in this problem. There is a way to obtain more regular foam components. For example, dry salt template synthesis provides a way to control the morphology of the metal foam, for example, using 2D^{26, 27} and 3D^{28, 29} salt templates.

What does this new synthesis mean to metal nano-foam research? We believe that it transforms the designing of a metal nano-foam—no longer a limited choice among given innate property of elements but choose from precursors whose availability is only a matter of engineering effort. Less noble metal elements, such as Cu, Ni or any elements whose salt precursors are available, can be tried to create a self-standing, mechanically stable nano-foam.

Conclusions

We showed the synthesis of an intermediate range Cu-Ni alloy nano-foam is possible via the electrospinning polymeric templated method with subsequent thermochemical processes. Oxide segregation and subsequent homogenization of the alloy nano-foam occurs during the decomposition and reduction step, respectively. The various polycrystalline compositions and morphologies were characterized by TEM, XRD, and SEM. The result demonstrates a way to bypass previous limits of materials selection set by innate electrochemical potential in metal nano-foam research, showing that metal elements with considerably different electrochemical potentials can form an alloy nano-foam given that their decomposable chemical precursors are available.

Acknowledgement

The authors gratefully acknowledge support from the National Science Foundation under Grant No. CMMI 1634772.

Supplementary Material Available: The measured interlayer spacings of the $\text{Cu}_{50}\text{Ni}_{50}$ alloy from the TEM diffraction patterns are tabulated in the supplementary material.

References

- 1. W. Luc and F. Jiao: Nanoporous metals as electrocatalysts: state-of-the-art, opportunities, and challenges. *ACS Catal.* **7**, 5856 (2017).
- J. Biener, A.M. Hodge, J.R. Hayes, C.A. Volkert, L.A. Zepeda-Ruiz, A.V. Hamza and F.F. Abraham: Size Effects on the Mechanical Behavior of Nanoporous Au. *Nano. Lett.* 6, 2379 (2006).
- 3. A. Neogi, L. He and N. Abdolrahim: Atomistic simulations of shock compression of single crystal and core-shell Cu@ Ni nanoporous metals. *Jpn. J. Appl. Phys.* **126**, 015901 (2019).
- 4. J. Biener, G.W. Nyce, A.M. Hodge, M.M. Biener, A.V. Hamza and S.A. Maier: Nanoporous plasmonic metamaterials. *Advanced Materials* **20**, 1211 (2008).
- 5. I. McCue, E. Benn, B. Gaskey and J. Erlebacher: Dealloying and dealloyed materials. *Annual review of materials research* **46**, 263 (2016).
- 6. M. Stratmann and M. Rohwerder: Materials science: A pore view of corrosion. *Nature* **410**, 420 (2001).
- 7. J. Erlebacher: An atomistic description of dealloying porosity evolution, the critical potential, and rate-limiting behavior. *J. Electrochem. Soc.* **151**, C614 (2004).

- 8. M. Hakamada and M. Mabuchi: Fabrication, Microstructure, and Properties of Nanoporous Pd, Ni, and Their Alloys by Dealloying. *Crit. Rev. Solid State Mater. Sci.* **38**, 262 (2013).
- 9. G.G. Li and H. Wang: Dealloyed nanoporous gold catalysts: from macroscopic foams to nanoparticulate architectures. *ChemNanoMat* **4**, 897 (2018).
- 10. A. Hodge, R. Doucette, M. Biener, J. Biener, O. Cervantes and A. Hamza: Ag effects on the elastic modulus values of nanoporous Au foams. *Journal of Materials Research* **24**, 1600 (2009).
- 11. C.-E. Kim, R.M. Rahimi, N. Hightower, I. Mastorakos and D.F. Bahr: Synthesis, microstructure, and mechanical properties of polycrystalline Cu nano-foam. *MRS Adv.* **3**, 469 (2018).
- 12. J. Zhang, M.D. Baró, E. Pellicer and J. Sort: Electrodeposition of magnetic, superhydrophobic, non-stick, two-phase Cu–Ni foam films and their enhanced performance for hydrogen evolution reaction in alkaline water media. *Nanoscale* **6**, 12490 (2014).
- 13. A. Greiner and J.H. Wendorff: Electrospinning: a fascinating method for the preparation of ultrathin fibers. *Angew. Chem. Int. Ed.* **46**, 5670 (2007).
- 14. J. Liu, M.J. Chang and H.L. Du: Facile preparation of cross-linked porous poly(vinyl alcohol) nanofibers by electrospinning. *Mater. Lett.* **183**, 318 (2016).
- 15. B.M. Eick and J.P. Youngblood: SiC nanofibers by pyrolysis of electrospun preceramic polymers. *J. Mater. Sci.* **44**, 160 (2009).
- 16. P.J. Spencer and W. Slough: Applied and Experimental Chemical Thermodynamics at High Temperatures. *High Temp-High Press* **2**, 123 (1970).
- 17. W.C. Oliver and G.M. Pharr: An improved technique for determining hardness and elastic modulus using load and displacement sensing indentation experiments. *J. Mater. Res.* 7, 1564 (1992).
- 18. W.C. Oliver and G.M. Pharr: Measurement of hardness and elastic modulus by instrumented indentation: Advances in understanding and refinements to methodology. *J. Mater. Res.* 19, 3 (2004).
- 19. D.F. Bahr and D.J. Morris: Nanoindentation: Localized probes of mechanical behavior of materials, (Springer2008).
- 20. S. Divinski, J. Ribbe, G. Schmitz and C. Herzig: Grain boundary diffusion and segregation of Ni in Cu. *Acta Materialia* **55**, 3337 (2007).
- 21. E.-a. Zen: Validity of "vegard's law", (Mineralogical Society of America 1956).
- 22. A.R. Denton and N.W. Ashcroft: Vegard's law. *Physical review A* 43, 3161 (1991).
- J. Erlebacher, M.J. Aziz, A. Karma, N. Dimitrov and K. Sieradzki: Evolution of nanoporosity in dealloying. *Nature* **410**, 450 (2001).
- 24. W. Weisweiler: KINETIC STUDIES OF THE CATALYTIC GRAPHITIZING OF GLASS-LIKE CARBON WITH THE AID OF NICKEL. *HIGH TEMP HIGH PRESSURES* **2**, 187 (1970).
- 25. M. Ashby: The properties of foams and lattices. *Philosophical Transactions of the Royal Society A: Mathematical, Physical and Engineering Sciences* **364**, 15 (2006).
- 26. X. Xiao, H. Yu, H. Jin, M. Wu, Y. Fang, J. Sun, Z. Hu, T. Li, J. Wu and L. Huang: Salt-templated synthesis of 2D metallic MoN and other nitrides. *ACS nano* 11, 2180 (2017).
- 27. X. Xiao, H. Song, S. Lin, Y. Zhou, X. Zhan, Z. Hu, Q. Zhang, J. Sun, B. Yang and T. Li: Scalable salt-templated synthesis of two-dimensional transition metal oxides. *Nature communications* 7, 1 (2016).
- 28. F.J. Burpo, E.A. Nagelli, A.R. Losch, J.K. Bui, G.T. Forcherio, D.R. Baker, J.P. McClure, S.F. Bartolucci and D.D. Chu: Salt-Templated Platinum-Copper Porous Macrobeams for Ethanol Oxidation. *Catalysts* **9**, 662 (2019).
- 29. F.J. Burpo, E.A. Nagelli, A.N. Mitropoulos, S.F. Bartolucci, J.P. McClure, D.R. Baker, A.R. Losch and D.D. Chu: Salt-templated platinum-palladium porous macrobeam synthesis. *MRS Communications* **9**, 280 (2019).

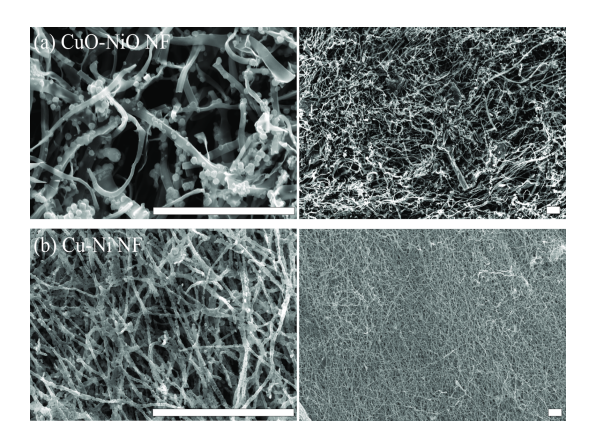


Figure 1: SEM images of the nanofoams in (a) oxide and (b) reduced metal phase. The scale bars are $10~\mu m$. The oxide phase features numerous granular segregations, which we identify as Cu-rich phase. These granular features disappear after reduction, presumably due to intermetallic diffusion between Cu and Ni.

15

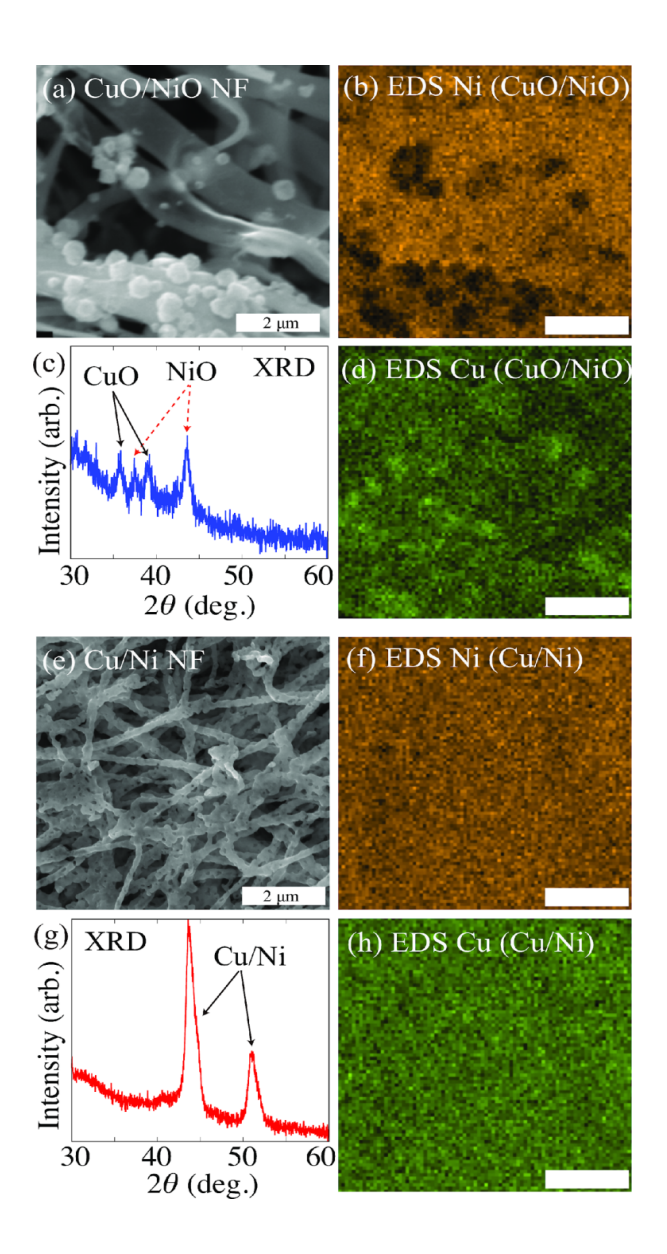


Figure 2: EDS mapping and XRD patterns of the (a-d) oxide and (e-h) reduced metal phase. The scale bars are 2 μm. The granular features of (a) is a Cu-rich oxide phase as shown in (d). After reduction, these granular features and XRD CuO peaks disappear, indicating reduction and intermetallic alloying proceeded simultaneously. The feature size of ligaments changed from oxide to metal phase, showing shrinkage occurs during the reduction process.

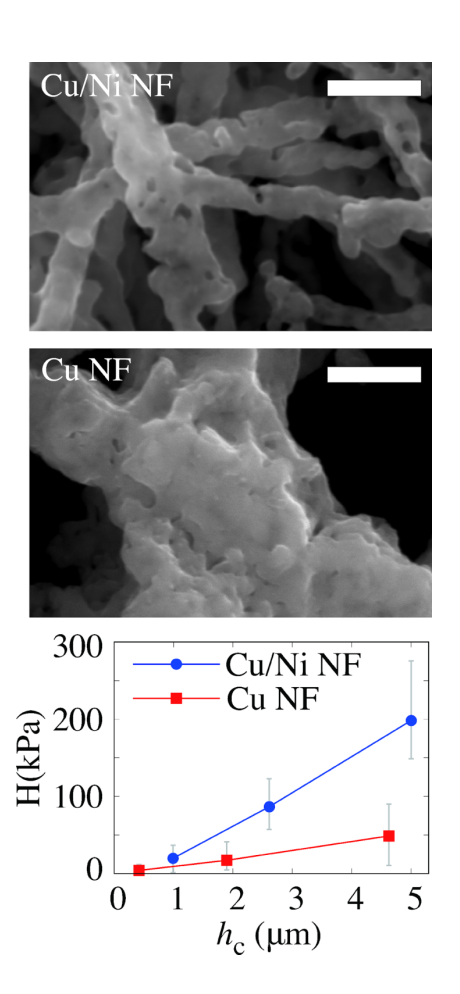


Figure 3: High resolution SEM images of the alloy nano-foam (top) compared to that of the previously reported single component Cu nano-foam (middle). 11 H denotes hardness which is the measured force divided by the contact area (area of the flat punch tip), and h_c denotes the contact depth that indicates how deep the indenter tip pushed down into the sample. The scale bars are 500 nm. The hardness, as measured by nanoindentation, of this Cu-Ni alloy nano-foam is about three times stronger than that of the single component Cu nano-foam.

17

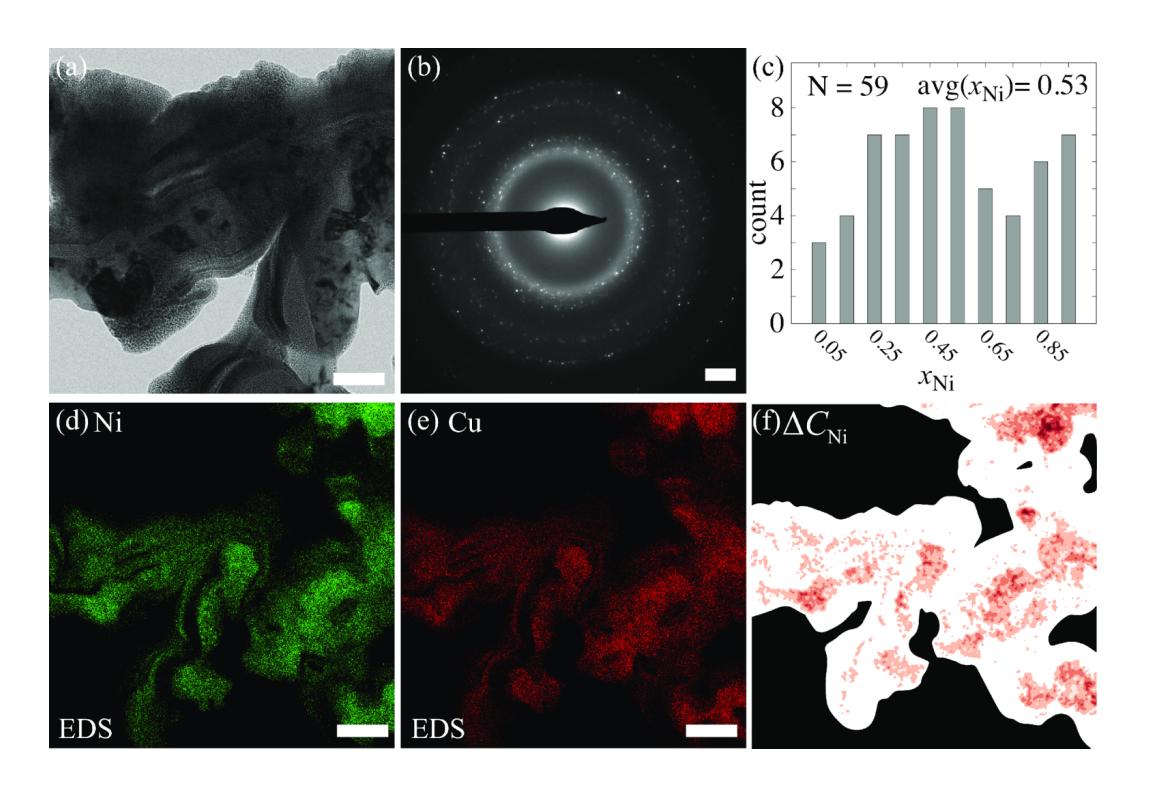


Figure 4: TEM analyses indicate the polycrystalline nature of the Cu-Ni alloy nanofoam. The (a) bright field image and (b) selected area diffraction shows polycrystallinity. The (c) Ni contents corresponding to individual grains are determined based on the Vegard's law.[ADD A CITATION] (d, e) EDS maps and (f) the segregation analysis computed using the two EDS maps. Atomic concentration difference ΔC of i th element is divided by the sum of total atomic concentration at given (x, y) point on the map, i.e. $\Delta C_{\text{Ni}} = C_{\text{Ni}} - C_{\text{Cu}}$ and $\Delta C_{\text{Cu}} = C_{\text{Cu}} - C_{\text{Ni}}$. For example, Ni +20% on the map means, the segregated, excessive amount of Ni at the point on the map is as large as 20% of the sum of all atomic concentration at the point. Note that using relative scale normalized the atomic concentration, making low-intensity region more visible than how it was in the original EDS map. Scalebars are 100 nm in (a,d,e), and 2 nm⁻¹ in (b).